Digest Journal of Nanomaterials and Biostructures Vol. 7, No. 4, October-December 2012, p. 1869-1880

COMPARATIVE STUDY OF THE PERFORMANCE CHARACTERISTICS OF GREEN InGaN SQW LASER DIODES WITH TERNARY AlGaN AND QUATERNARY AlInGaN ELECTRON BLOCKING LAYER

GH. ALAHYARIZADEH*, Z. HASSAN, S.M. THAHAB[a], M. AMIRHOSEINY,
N. NADERI
Nano-Optoelectronics Research and Technology Laboratory, School of Physics,
University Science USM, Malaysia, 11800- Penang, Malaysia
[b]*Material Engineering Department, College of Engineering, University of Kufa,*
Najaf, Iraq

The effect of built-in polarization on the performance characteristics of green InGaN single quantum well (SQW) laser diode (LD) structures with ternary AlGaN or quaternary AlInGaN electron blocking layer (EBL) having the same bandgap energy, was investigated numerically. Simulation results indicated that using quaternary AlInGaN EBL effectively improves the performance characteristics of green InGaN SQW LDs. Using AlInGaN EBL significantly reduces the built-in polarization and fixed polarization charge densities at the EBL and the last InGaN barrier interface. Furthermore, using quaternary AlInGaN EBL increases the radiative recombination and decreases the non-radiative recombination in the well. The laser structure with AlInGaN EBL has lower threshold current, and higher output power, differential quantum efficiency (DQE) and slope efficiency compared with the laser structure with conventional AlGaN EBL.

(Received September 24, 2012; Accepted November 28, 2012)

Keywords: Green InGaN laser diode, AlInGaN, Electron blocking layer,
Built-in polarization, Numerical simulation

1. Introduction

III-nitride-based green semiconductor laser diodes (LDs) have recently attracted much attention because of their essential application in full-color projectors, envisioned for introduction to the market in the future. III-nitride-based green LDs promise potential reduction in production costs, compactness, wider wavelength range access, and increased efficiency and reliability [1–3].

After the first demonstration of blue InGaN laser diodes by Nakamura et al. [4], several groups such as Ryu et al. [5], Kuo et al. [6], and others investigated and developed III-nitride laser diodes to achieve lower (violet and ultraviolet) and longer (green) wavelengths experimentally and theoretically using different equipment and methods separately [6–10]. To follow this trend, in recent years, several researchers have published their results on longer wavelength laser diodes at 500 nm to 530 nm [1–4, 10–17]. Although these laser diodes have been realized by several groups, InGaN green lasers is an emerging subject, and few studies have been carried out in terms of carrier behaviour and investigation of structural, optical, and electrical parameters affecting laser performance. Furthermore, the tendency of green laser diodes to reach greater performance and lower threshold current encourages researchers to continue investigating these diodes theoretically and experimentally.

Built-in electrostatic fields related to strain, piezoelectric and spontaneous polarizations play a very significant role in III-nitride based devices [18]. Piezoelectric and spontaneous

---

* Corresponding author: g_alahyarizadeh@yahoo.com

polarizations are inherent problems in GaN-based alloys, which limit the development of III-nitride based optoelectronic devices [19]. The built-in electrostatic field causes strong deformation of quantum wells and their adjoining layers, resulting in separate electron and hole wave functions in quantum wells that lead to the decrease in photon emission rate and quantum efficiency [19, 20]. Built-in polarization and, consequently, built-in electric field due to large polarization charges at the InGaN barrier and the AlGaN electron blocking layer (EBL) interface is an important issue that significantly influences laser threshold current [21].

Using quaternary AlInGaN layer instead of AlGaN is one of the methods employed in controlling built-in polarization and electrostatic field. Choosing an appropriate Al and In composition in the quaternary AlInGaN layers allows the possibility of controlling both piezoelectric and spontaneous polarizations [19]. Quaternary alloys also offer excellent potential for fabrication of lattice-matched III-nitride layers by controlling the bandgap energy and lattice parameter [22]. Many studies have concentrated on using quaternary AlInGaN EBL, instead of ternary AlGaN EBL, in the laser structures. Experimental studies in various areas, such as ultraviolet [23], violet wavelength near 405 nm [22–24], violet wavelength near 415 nm [25], and blue wavelength [26] indicated that using quaternary AlInGaN EBL significantly improves laser performance and decreases laser threshold current.

In the current research, a comparative study on the performance characteristics of green InGaN single quantum well (SQW) LDs employing a ternary AlGaN and a quaternary AlInGaN EBL having output emission wavelengths from 500 nm to 510 nm was conducted using Integrated System Engineering Technical Computer Aided Design (ISE TCAD) software. The distribution of the electron and hole carrier densities, radiative recombination, as well as their roles on laser performance for both structures were also presented. The built-in polarization effects due to the use of ternary AlGaN and quaternary AlInGaN EBL at the laser InGaN barrier and EBL interface were also investigated.

2. Laser structure and simulation parameters

The fundamental laser structure under study was extracted from a real laser structure fabricated by Adachi et al., which was grown through metal organic chemical vapour deposition [1, 2]. As shown in Fig. 1., the optimized quantum well laser structure which is used in the study includes an n-type GaN layer, an n-type InGaN compliance layer, an n-type AlInGaN quaternary cladding layer, an n-type GaN waveguiding layer, an InGaN/InGaN SQW active region, a p-type $Al_{0.2}Ga_{0.8}N$ electron blocking layer (EBL), a p-type GaN waveguiding layer, a p-type AlInGaN quaternary cladding layer, and a p-type GaN contact layer [1, 2]. The SQW active region was selected based on Nakamura et al., which consists of a 4 nm $In_{0.3}Ga_{0.7}N$ wells sandwiched between two 10 nm $In_{0.03}Ga_{0.97}N$ barriers [3]. The doping concentrations of n- and p-type layers are 1e18 and 5.5e18, respectively. The laser area is 3 µm×350 µm, and the reflectivities of the back and front mirrors are equal to 80% and 95%, respectively [1,2].

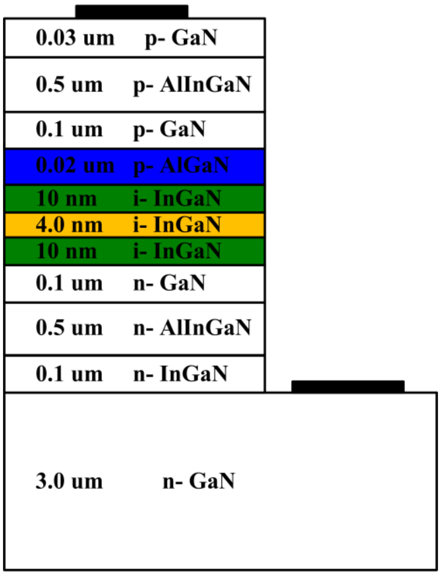

Fig. 1. Schematic diagram of the green InGaN SQW laser structure under study

Several sets of equations, including the Schrodinger, Poisson, photon-rate, current continuity, and scalar wave equations, were solved in the laser simulation process using the two-dimensional ISE TCAD simulator. The ISE TCAD simulator also includes a carrier drift-diffusion model that contains Fermi statistics and incomplete ionization [12].

The physical parameters of the ternary and the quaternary alloys used in the simulation were interpolated by binary alloys that can be expressed by the following equation:

$$Q_{Al_xIn_yGa_{1-x-y}N} = x \cdot Q_{AlN} + y \cdot Q_{InN} + (1-x-y) \cdot Q_{GaN}, \tag{1}$$

where Q_{InN}, Q_{GaN}, and Q_{AlN} are the physical parameters of InN, GaN, and AlN, such as effective masses, refractive index, and others as listed in Table 1 [8, 12]. The above equation applies to all physical parameters except for band gap energy, which can be expressed by the following equations [8,12]:

$$E_g(AlInGaN) = \frac{xyE_g^u(AlInN) + yzE_g^v(InGaN) + xzE_g^w(AlGaN)}{xy + yz + zx}, \tag{2}$$

$$E_g^u(AlInN) = u \cdot E_g(InN) + (1-u) \cdot E_g(AlN) - u \cdot (1-u) b(AlInN), \tag{3}$$

$$E_g^v(InGaN) = v \cdot E_g(GaN) + (1-v) \cdot E_g(InN) - v \cdot (1-v) b(InGaN), \tag{4}$$

$$E_g^w(AlGaN) = w \cdot E_g(GaN) + (1-w) \cdot E_g(AlN) - w \cdot (1-w) b(AlGaN), \tag{5}$$

$$u = \frac{1-x+y}{2}, \quad v = \frac{1-y+z}{2}, \quad w = \frac{1-x+z}{2}, \tag{6}$$

where x, y, and $z = 1 - x - y$ are the compositions of aluminium, indium, and gallium in the AlInGaN, respectively. $E_g(InN)$, $E_g(GaN)$, and $E_g(AlN)$ are the band gap energies of InN, GaN, and AlN, respectively, while *b(AlInN)*, *b(InGaN)*, and *b(AlGaN)* are band gap bowing parameters of AlInN, InGaN, and AlGaN which are 2.5, 1.4, and 0.7, respectively [12].

Built-in polarization, induced in the III-nitride materials due to spontaneous and piezoelectric polarizations, is a problem that affects laser performance and must not be neglected. The spontaneous polarization of ternary and quaternary III-nitride alloys can be calculated using Eq. (2). The spontaneous polarization of ternary III-nitride alloys can also be expressed by the following equations [3, 10, 12, 16]:

$$P_{sp}(Al_xGa_{1-x}N) = -0.090x - 0.034(1-x) + 0.019x(1-x) \tag{7}$$

$$P_{sp}(In_xGa_{1-x}N) = -0.042x - 0.034(1-x) + 0.038x(1-x) \tag{8}$$

$$P_{sp}(Al_xIn_{1-x}N) = -0.090x - 0.042(1-x) + 0.071x(1-x) \tag{9}$$

The piezoelectric polarization of ternary and quaternary III-nitride alloys can be estimated by the following expression [3,10,16]:

$$P_{pz}(Al_xIn_yGa_{1-x-y}N) = x \cdot P_{pz}(AlN) + y \cdot P_{pz}(InN) + (1-x-y) \cdot P_{pz}(GaN) \tag{10}$$

where

$$P_{pz}(AlN) = -1.808\varepsilon + 5.624\varepsilon^2, \qquad for \quad \varepsilon < 0 \tag{11}$$

$$P_{pz}(AlN) = -1.808\varepsilon - 7.888\varepsilon^2, \qquad for \quad \varepsilon > 0 \tag{12}$$

$$P_{pz}(GaN) = -0.918\varepsilon + 9.541\varepsilon^2 \tag{13}$$

$$P_{pz}(InN) = -1.373\varepsilon + 7.559\varepsilon^2 \tag{14}$$

$$\varepsilon = (a_0 - a_a)/a_a \tag{15}$$

where $\varepsilon = \varepsilon_{xx} = \varepsilon_{yy}$ is the epitaxial growth plane strain tensor, which has an important function when layers are grown on top of each. a_0 and a_a are the lattice constants of the substrate and the top epitaxial layers, respectively. The perpendicular strain tensor can also be calculated by the following equation [3, 10, 12, 16]:

$$\varepsilon_{zz} = -\frac{2C_{13}}{C_{33}}\varepsilon_{xx} \tag{16}$$

where C_{13} and C_{33} are the elastic stiffness constants.

The total polarization of the layer can be estimated as

$$P_{total}(Al_xIn_yGa_{1-x-y}N) = P_{sp}(Al_xIn_yGa_{1-x-y}N) + P_{pz}(Al_xIn_yGa_{1-x-y}N) \tag{17}$$

At the abrupt interface of a top/bottom layer heterostructure, total polarization causes a fixed polarization charge and, consequently, an electric field, which depends on the top- and bottom-layer thicknesses.

$$\sigma = (P_{tot}^b - P_{tot}^t)(L_t + L_b)/(L_t\varepsilon_b + L_b\varepsilon_t) \tag{18}$$

$$F_t = L_b(P_{tot}^b - P_{tot}^t)/[\varepsilon_0(L_t\varepsilon_b + L_b\varepsilon_t)] \tag{19}$$

where P_{tot}^t and P_{tot}^b are the total polarization, L_t and L_b are the thicknesses, and ε_t and ε_b are the relative dielectric constants of the top and bottom layers, respectively, which can be interpolated by binary alloys [3,12, 20, 21]. The binary materials parameters used in this work are listed in Table 1 [12].

Table 1. Room temperature properties of binary III-N materials [12]

Parameters	GaN	AlN	InN
Bandgap energy E_g (eV)	3.47	6.28	0.8
Electron affinity (eV)	4.1	1.9	5.8
Lattice constant $a_o(°A)$	3.189	3.112	3.545
Refractive index near E_g	2.506	2.035	2.9
Electron effective mass	0.22 m_e	0.4 m_e	0.11m_e
Heavy hole effective mass	1.595 m_e	2.68 m_e	1.449 m_e
Light hole effective mass	0.261 m_e	0.261 m_e	0.157 m_e

3. Simulation results and discussion

Fig. 2 shows the spontaneous polarization, piezoelectric polarization, and the total polarization charges as a function of Al or In mole fraction of the ternary AlGaN and InGaN layers grown on a typical GaN layer. The AlGaN and InGaN epitaxial layers have tensile and compressive strains, respectively, compared with a typical GaN layer. The piezoelectric polarization behaviours of AlGaN and InGaN with increasing Al and In mole fractions are opposite. Although the spontaneous polarization of both AlGaN and InGaN show the same behaviours (negative), the total polarization behaviour of AlGaN and InGaN is the same as the piezoelectric polarization. Therefore, choosing an appropriate Al and In composition as quaternary AlInGaN alloy can control the built-in polarization at the interface of the AlInGaN layer and InGaN or GaN layer.

Using the quaternary AlInGaN EBL instead of the ternary AlGaN EBL is one of the methods employed in increasing laser performance. By choosing appropriate Al and In composition in the quaternary AlInGaN EBL, the built-in polarization effects and the strain can be controlled. To investigate the effect of quaternary EBL on the performance characteristics of InGaN green SQW laser, the ternary $Al_{0.2}Ga_{0.8}N$ EBL was replaced with quaternary AlInGaN EBL with Al composition from 0.22 to 0.32 and with the corresponding In composition having EBLs with bandgap energy identical to that of $Al_{0.2}Ga_{0.8}N$ EBL (Fig. 3).

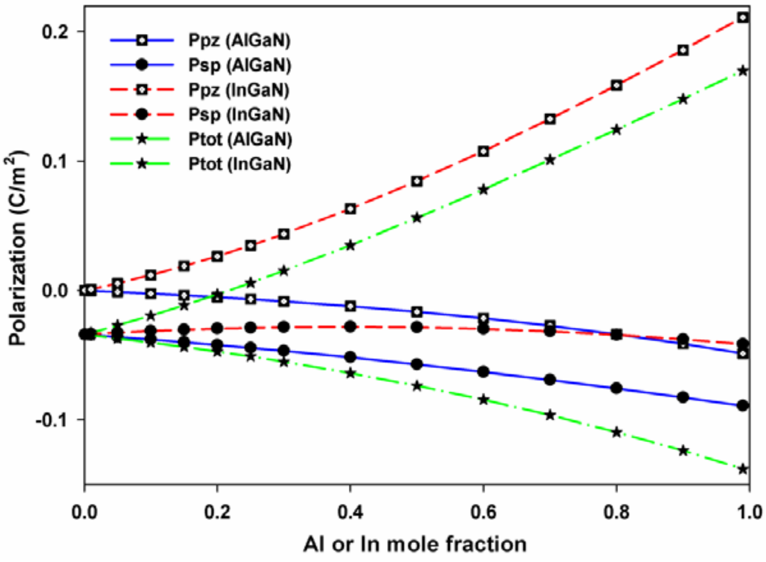

Fig. 2. Spontaneous polarization, piezoelectric polarization and total polarization charges as a function of Al or In mole fraction of the ternary AlGaN and InGaN layers grown on a typical GaN layer.

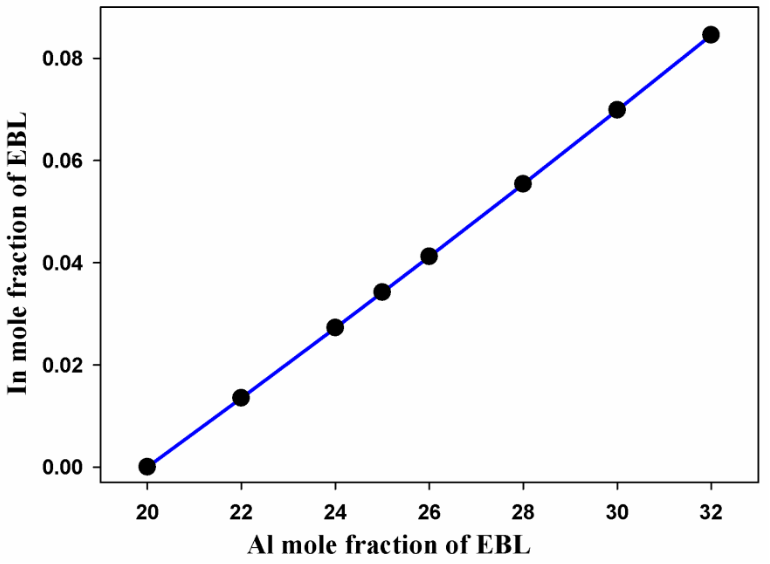

Fig. 3. In mole fraction of quaternary AlInGaN EBL as a function of Al mole fraction to attain a 3.92 eV bandgap of $Al_{0.2}Ga_{0.8}N$ *EBL*

Fig. 4 shows the spontaneous polarization, piezoelectric polarization, total polarization, and polarization charge densities at the EBL and last InGaN barrier interface as a function of Al mole fraction of the quaternary AlInGaN EBL. Fig. 4 (a)–(c) shows that increasing the Al mole fraction increases the In mole fraction spontaneous polarization and decreases the piezoelectric and total polarizations. The piezoelectric polarization decreases with the increase in the Al mole fraction of quaternary EBL up to 0.29; it increases again thereafter. Fig. 4(d) shows that the polarization charge densities at the EBL and last InGaN barrier interface decrease with the increase in Al mole fraction. Fig. 5 shows the strain at the EBL and last InGaN barrier interface as a function of the Al mole fraction of quaternary AlInGaN EBL. A compressive strain is observed in the ternary $Al_{0.2}Ga_{0.8}N$ EBL, which decreases with the use of quaternary AlInGaN EBL with Al mole fraction from 0.22 to 0.29. The strain becomes tensile and increases when the Al mole fraction of quaternary EBL is increased to more than 0.29.

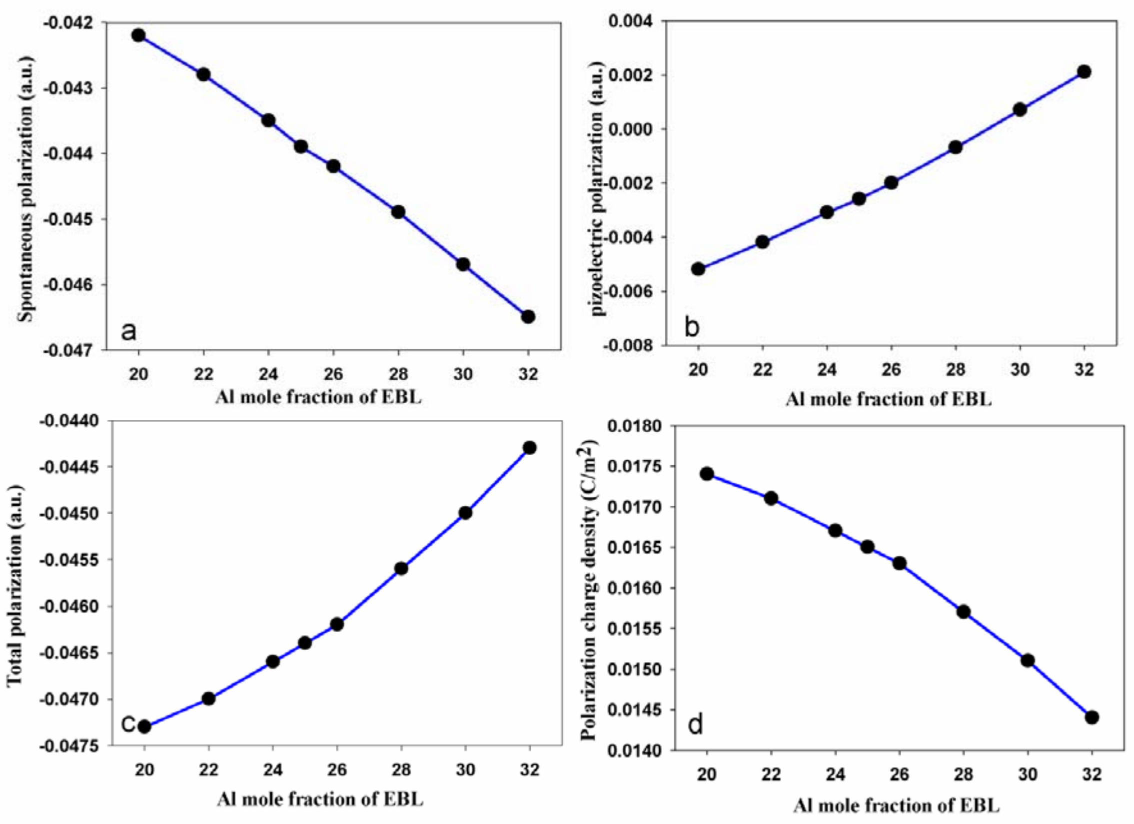

Fig. 4. Spontaneous polarization, piezoelectric polarization, total polarization, and polarization charge densities at the EBL and last InGaN barrier interface as a function of Al mole fraction of the quaternary AlInGaN EBL.

The quaternary AlInGaN EBL with a 0.25 Al mole fraction was used in the laser structure based on the built-in polarization effects, polarization charges, and resulting electric fields. Fig. 6 shows the conduction- and valence-band energies and the electron and hole Fermi levels of the InGaN green SQW lasers with ternary AlGaN and quaternary AlInGaN EBL. The slightly deformed conduction-band profile near the quaternary AlInGaN EBL and the last InGaN barrier interface is due to the decreasing polarization charge densities and their corresponding electric fields. Lower electron accumulation is observed when quaternary AlInGaN EBL is used compared with the use of ternary AlGaN EBL. The valence-band profile is also deformed near the quaternary AlInGaN EBL and the last InGaN barrier interface, which results in higher hole accumulation.

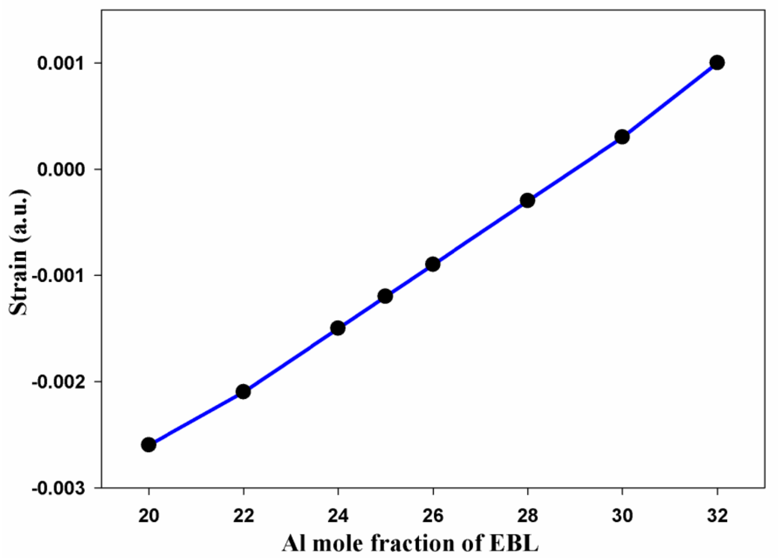

Fig. 5. Strain interface of EBL and last InGaN barrier as a function of Al mole fraction of quaternary AlInGaN EBL.

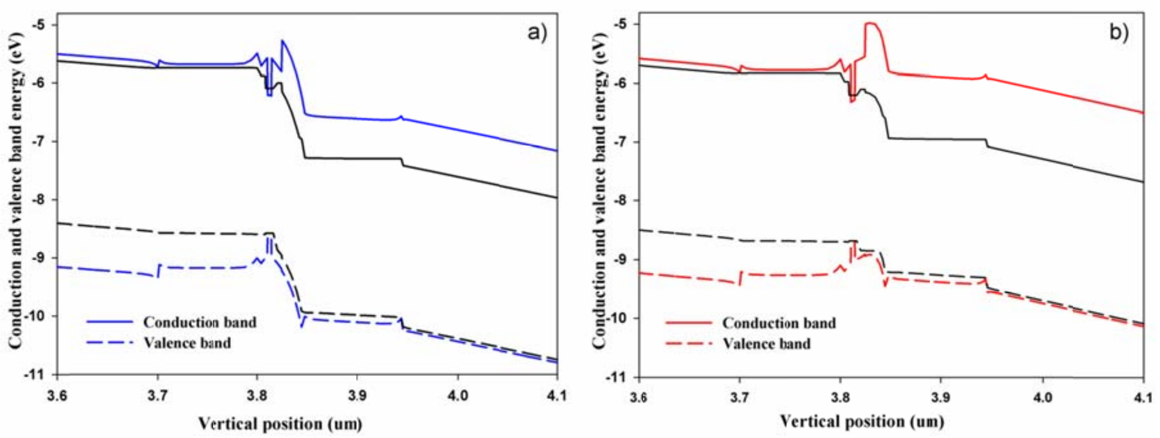

Fig. 6. Conduction- and valence- band energies of InGaN green SQW lasers with (a) ternary AlGaN and (b) quaternary AlInGaN EBL

The electron and hole densities of green InGaN SQW LDs with ternary AlGaN and quaternary AlInGaN EBL are shown in Fig. 7. The deformation in the conduction and valence bands due to reduced built-in electric field using quaternary EBL changes the electron and hole densities in the well. Increasing the hole concentration in the well, as well as considering their longer escape time due to their higher mass compared with electrons, causes higher radiative electron–hole recombination in the well. Fig. 8 shows the radiative, non-radiative, and total recombination rates for green InGaN SQW LDs with ternary AlGaN and quaternary AlInGaN EBL. Using the quaternary AlInGaN EBL increases the radiative electron and hole recombination, decreases non-radiative recombination, and increases the total recombination in the well. Increasing the radiative electron and hole recombination in the well decreases the number of electrons escaping from the well and injected to the p-side region. Therefore, the electron current injected in the well is reduced through recombination with the hole, and the electron current overflow of the well to the p-side region is reduced.

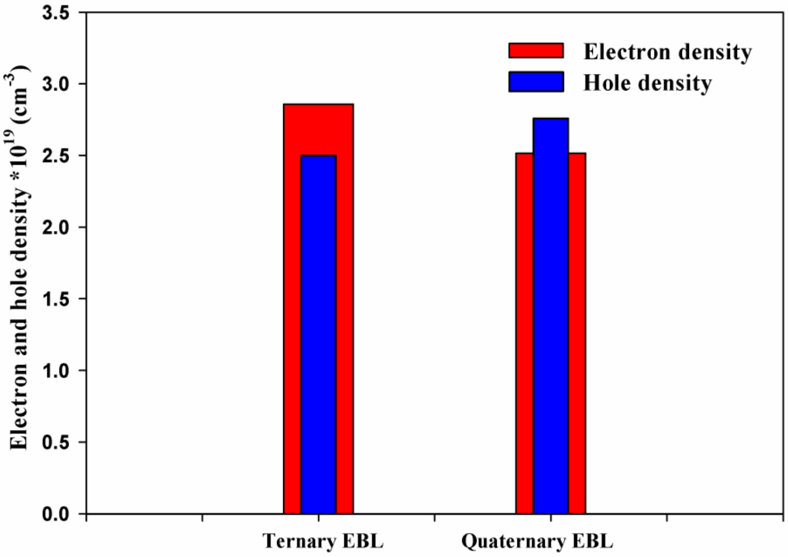

Fig. 7. Electron and hole densities of green InGaN SQW LDs with ternary AlGaN and quaternary AlInGaN EBL

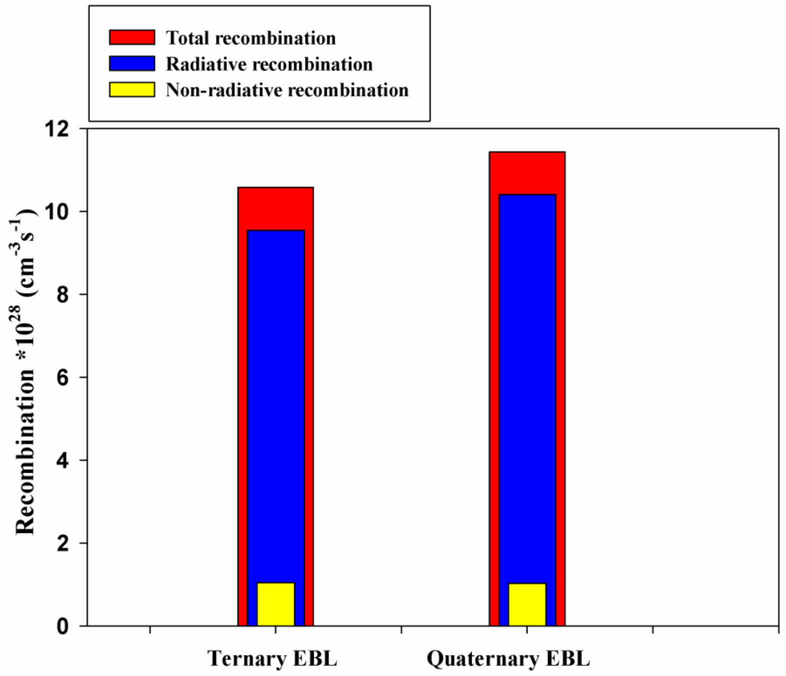

Fig. 8. Radiative, non-radiative, and total recombination rates for green InGaN SQW LDs with ternary AlGaN and quaternary AlInGaN EBL

Enhancing radiative recombination in the well using the quaternary AlInGaN EBL also increases the optical output power. On the other hand, using the quaternary AlInGaN EBL increases the optical confinement factor (OCF) because of more carrier accumulation in the active region. The increase in OCF and optical output power as optical intensity is shown in Fig. 9.

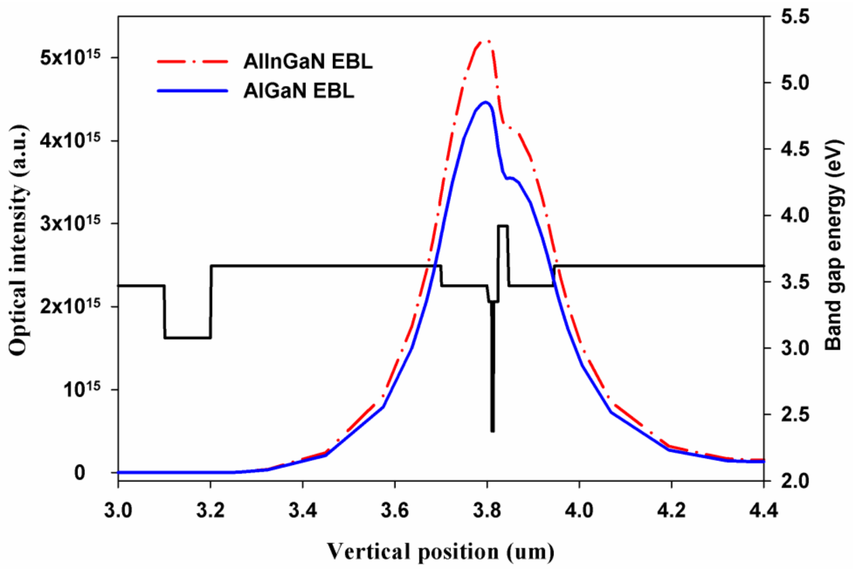

Fig. 9. Optical intensity and bandgap energy profile of green InGaN SQW LDs with a ternary AlGaN and a quaternary AlInGaN EBL.

Fig. 10 shows the light–current (*L*–*I*) and voltage–current (*V*-*I*) characteristics of the green InGaN SQW lasers with ternary AlGaN and quaternary AlInGaN EBL. Using the quaternary AlInGaN EBL significantly decreases the laser threshold current compared with that using AlGaN EBL because of reduced electron current overflow from the active region to the p-side region. Employing quaternary AlInGaN EBL also increases the output power, slope efficiency, and external quantum efficiency compared with using AlGaN EBL. The performance characteristics of the green InGaN SQW lasers with ternary AlGaN and quaternary AlInGaN EBL are summarized in Table 2.

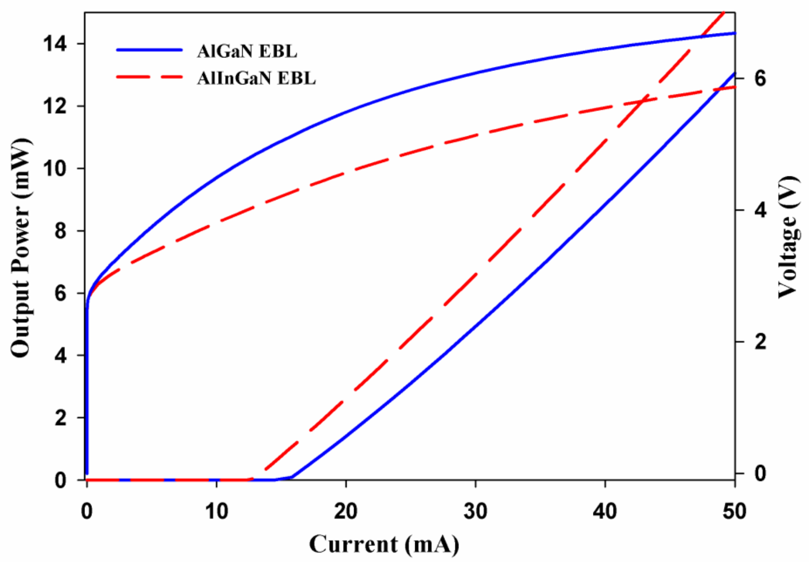

Fig. 10. L–I and V–I characteristics of the green InGaN SQW lasers with ternary AlGaN and quaternary AlInGaN EBL

Table 2. Threshold current, slope efficiency, output power, and DQE of the green InGaN SQW LDs with ternary AlGaN and quaternary AlInGaN EBL.

EBL	**Threshold current (mA)**	**Slope efficiency (W/A)**	**Output power (mW)**	**DQE (%)**
AlGaN	15.539	0.444	27.134	36.327
AlInGaN	12.797	0.464	29.811	38.087

Figure 11 shows the threshold current and output power of the green InGaN SQW laser as a function of Al mole fraction of EBL. Using the quaternary EBL significantly decreases the threshold current and increases the output power. Increasing the Al mole fraction results in slightly higher output power and lower threshold current.

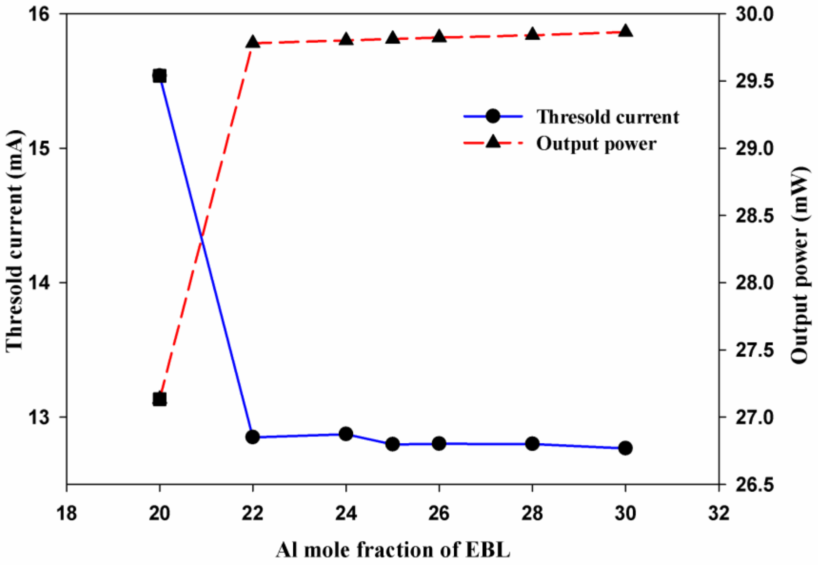

Fig. 11. Threshold current and output power of the green InGaN SQW laser as a function of Al mole fraction of EBL.

4. Conclusion

The performance characteristics of green InGaN SQW LDs employing ternary AlGaN and quaternary AlInGaN EBL with emission wavelengths from 500 nm to 510 nm have been investigated using ISE TCAD software. Simulation results indicated that using quaternary AlInGaN EBL significantly reduces the built-in polarization and polarization charge density at the EBL and InGaN barrier interface and also effectively improves the performance characteristics of green InGaN SQW LDs. Moreover, using the quaternary AlInGaN EBL increases radiative recombination and decreases non-radiative recombination in the active region. The laser structure with AlInGaN EBL has a lower threshold current and higher output power, differential quantum efficiency, and slope efficiency compared with the laser structure using conventional AlGaN EBL.

Acknowledgment

The support from RU grant and Universiti Sains Malaysia is gratefully acknowledged.

References

[1] Y. Yoshizumi, M. Adachi, Y. Enya, T. Kyono, S. Tokuyama, T. Sumitomo, K. Akita, T. Ikegami, M. Ueno, K. Katayama, T. Nakamura, Applied Physics Express, **2**(9), 092101 (2009).

[2] M. Adachi, Y. Yoshizumi, Y. Enya, T. Kyono, T. Sumitomo, S. Tokuyama, S. Takagi, K. Sumiyoshi, N. Saga, T. Ikegami, M. Ueno, K. Katayama, and T. Nakamura, Applied Physics Express, **3**, 121001 (2010).

[3] A. Tyagi, R. M. Farrell, K. M. Klchner, C. Y. Huang, P. S. Hsu, D. A. Haeger, M. T. Hardy, C. Holder, K. Fujito, D. A. Cohen et al., Applied Physics Express, **3**, 011002 (2010).

[4] Y.-D. Lin, A. Chakraborty, S. Brinkley, H. C. Kuo, T. Melo, K. Fujito, J. S. Speck, S. P. DenBaars, and S. Nakamura, Applied Physics Letters, **94**, 261108-3 (2009).

[5] H. Y. Ryu, K. H. Ha, J. K. Son, S. N. Lee, H. S. Paek, T. Jang, Y. J. Sung, K. S. Kim, H. K. Kim, Y. Park, and O. H. Nam, Applied Physics Letters, **93**, 011105-3 (2008).

[6] Y. Chang and Y.K. Kuo, Journal of Applied Physics, **93**, 4992 (2003).

[7] T. Lermer, A. Gomez-Iglesias, M. Sabathil, J. Muller, S. Lutgen, U. Strauss, B. Pasenow, J. Hader, J. V. Moloney, S. W. Koch, W. Scheibenzuber, U. T. Schwarz, Applied Physics Letters, **98**, 021115-3 (2011).

[8] Gh. Alahyarizadeh, A. J. Ghazai, R. Rahmani, H. Mahmodi, Z. Hassan, Optics Communications, **285**, 746 (2012).

[9] Y. K. Kuo, B. T. Liou, M. L. Chen, S. H. Yen, C. Y. Lin, Optics Communications, **231**, 395 (2004).

[10] D. S. Sizov, R. Bhat, A. Zakharian, S. Kechang, D. E. Allen, S. Coleman, Z. Chung-en, IEEE Journal of Selected Topics in Quantum Electronics, **17**, 1390 (2011).

[11] C.-Y. Huang, Y.-D. Lin, A. Tyagi, A. Chakraborty, H. Ohta, J. S. Speck, S. P. DenBaars, S. Nakamura, Journal of Applied Physics, **107**, 023101-7 (2010).

[12] Gh. Alahyarizadeh, Z. Hassan, S.M. Thahab, A.J. Ghazai, H. Mahmodi, Journal of nanophotonics, 2012, in press.

[13] D. Queren, A. Avramescu, G. Bruderl, A. Breidenassel, M. Schillgalies, S. Lutgen, U. Strauss, Applied Physics Letters, **94**, 081119-3 (2009).

[14] A. Avramescu, T. Lermer, J. Muller, S. Tautz, D. Queren, S. Lutgen, and U. Strauss, Applied Physics Letters, **95**, 071103-3 (2009).

[15] T. Miyoshi, S. Masui, T. Okada, T. Yanamoto, T. Kozaki, S. Nagahama, T. Mukai, Applied Physics Express, **2**, 062201 (2009).

[16] Y. Enya, Y. Yoshizumi, T. Kyono, K. Akita, M. Ueno, M. Adachi, T. Sumitomo, S. Tokuyama, T. Ikegami, K. Katayama, T. Nakamura, Applied Physics Express, **2**(8), 082101 (2009).

[17] D. S. Sizov, R. Bhat, A. Zakharian, J. Napierala, K. Song, D. Allen, C. Zah, Applied Physics Express, **3**, 122101 (2010).

[18] J. Zhang, J. Yang, G. Simin, M. Shatalov, M. A. Khan, M. S. Shur, R. Gaska, Applied Physics Letters, **77**, 2668 (2000).

[19] J.-R. Chen, C.-H. Lee, T.-S. Ko, Y.-A. Chang, T.-C. Lu, H.-C. Kuo, Y.-K. Kuo, S.-C. Wang, J. Lightwave Technol. **26**, 329 (2008).

[20] L. H. Peng, C. W. Chuang, L. H. Lou, Applied Physics Letters, **74**, 795 (1999).

[21] J. Piprek, R. Farrell, S. DenBaars, S. Nakamura, Photonics Technology Letters, IEEE, **18**, 7 (2006).

[22] R. A. Abdullah, K. Ibrahim, Optics Communications, **282**, 4755 (2009).

[23] A. J. Ghazai, S. M. Thahab, H. Abu Hassan, Z. Hassan, Opt. Express, **19**, 9245 (2011).

[24] Y.-K. Kuo, Y.-C. Lu, M.-C. Tsai, S.-H. Yen, presented at Physics and Simulation of Optoelectronic Devices XVII, San Jose, CA, USA, 2009.

[25] S. M. Thahab, H. A. Hassan, and Z. Hassan, World Academy of Science, Engineering ans Technology, vol. 55, 2009.

[26] Y.-K. Kuo, M.-C. Tsai, S.-H. Yen, Optics Communications, **282**, 4252 (2009).